Nano Energy 122 (2024) 109334

Contents lists available at ScienceDirect

Nano Energy

journal homepage: www.elsevier.com/locate/nanoen

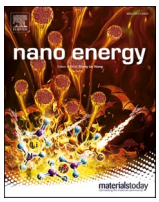

Textured nanofibers inspired by nature for harvesting biomechanical energy and sensing biophysiological signals

Sun Hwa Kwon, Chi Zhang, Zhipeng Jiang, Lin Dong *

Department of Mechanical and Industrial Engineering, New Jersey Institute of Technology, Newark, NJ 07102, USA

ARTICLE INFO

Keywords:
Porous nanofibers
Wrinkled nanofibers
Bioinspiration design
Piezoelectric
Energy harvesting
Biophysiological sensing

ABSTRACT

Flexible electronics are emerging as a promising new platform for wearables; however, their practical utility is hindered by the limited battery life of electronic devices and the need for frequent battery replacements. Here, we report self-powered, flexible, permeable, tough, and lightweight biomechanical energy harvesting and biophysiological sensing devices using textured nanofibers for wearable electronics applications. The textured structure draws inspiration from two major sources of nature: the interior porous structure of jute fibers and the rough bark texture of trees. Interior pores are introduced to the nanofibers to increase compressibility and breathability like jute fibers. The inspiration from the rough bark texture also leads to a wrinkled surface morphology of the nanofibers to expand the surface area and consequently enhance toughness. To design and fabricate such a textured structure, the vapor-induced phase separation mechanism and electrospinning technique are employed within a controllable high humidity environment. Consequently, the textured nanofiber-based devices exhibit a well-rounded performance in electrical, mechanical, and physical properties, specifically demonstrating a significantly enhanced piezoelectric performance with more than two-fold electrical generation. These textured devices not only effectively harvest biomechanical energy from human movement but also demonstrate sensing capability for self-powered multifunctional biophysiological monitoring applications by leveraging the same piezoelectric mechanism. The novel design strategy for the textured nanofibers and their resultant balanced performance promotes the versatility and practical applicability of piezoelectric fibrous energy harvesting and sensing devices, contributing to the development of next-generation flexible and wearable electronics.

1. Introduction

Flexible electronics have taken the world by storm over the past several decades due to their immense potential in a broad range of applications [1–6]. These flexible electronics provide novel approaches to design and manufacture wearables, enabling innovative solutions for the challenges in traditional electronics. However, the practical utility is compromised by the limited battery life of the electronic device and the requirement for periodic battery replacements, leading to an overall bulky device with limited long-term utilization, performance, and consideration of user comfort. Therefore, there is a critical need to optimize the power source of flexible electronics [1,7,8]. The human body, on the other hand, stands out as a substantial source of biomechanical energy, demonstrating potential for direct utilization in powering a variety of bioelectronic devices. For example, an average human body generates energy roughly equivalent to the output of 800 AA batteries (2500 mAh) [9–13]. By utilizing a method to harness the biomechanical energy that is continuously being generated both actively (such as joint movements and feet stepping on the ground) and passively (such as the heart beating and diaphragm movements), the essentially "free" energy could be harvested without it being dissipated into the ambient environment [2,14]. Piezoelectric materials have attracted a lot of interest in energy harvesting due to their ability to convert mechanical energy, including that generated by sources like the human body, into electrical power [15–17]. Among various piezoelectric materials, piezoelectric polymers such as polyvinylidene fluoride (PVDF) and its copolymer poly(vinylidene fluoride-trifluoroethylene) (P(VDF-TrFE)) are excellent candidates for flexible electronics due to their exceptional flexibility, biocompatibility, light weight, and great processability with micro/nano structures [18–22]. For example, PVDF and P(VDF-TrFE) can be designed and fabricated into nanostructures such as nanofibers [23–25], nanowires [26,27], nanotubes [28–30], and more to

* Corresponding author.
E-mail address: lin.dong@njit.edu (L. Dong).

https://doi.org/10.1016/j.nanoen.2024.109334
Received 21 November 2023; Received in revised form 10 January 2024; Accepted 22 January 2024
Available online 24 January 2024

demonstrate their excellent processability into a variety of structures without degrading their piezoelectrically active components. Moreover, piezoelectric polymers also have great chemical resistance and thermal stability that make them ideal for long-term wearable applications [18,21,22]. With the same working mechanism, piezoelectric polymeric devices that are used as energy harvesters can also function as self-powered sensors or transducers to demonstrate their versatility in other fields such as healthcare. Despite those desirable advantages, they display weak piezoelectric properties when compared to other piezoelectric materials such as ceramics and single crystals, posing challenges in achieving effective energy harvesting and advanced sensing capability [19,31,32].

Different material designs and fabrication methods have been explored to address such challenges that can improve the piezoelectric properties of polymers [27,33–37]. Notably, the electrospinning method stands out for its simple operation and versatility, enabling the use of a broad range of materials and the ability to control fibrous morphology and dimensions that can enhance the electrical properties of such polymers [22,24,38,39]. Essentially, the polymer solution undergoes a high voltage field and mechanical stretching to produce continuous and uninterrupted nanofibers of variable diameters that eventually solidify into conventional cylindrical structures with smooth surfaces [24,38]. The nanofibers are simultaneously polarized during fabrication, which can enhance the piezoelectricity of polymeric materials such as PVDF and its copolymer P(VDF-TrFE) during the fabrication process without further post-treatment [22,38,39]. In the electrospinning approach, the mechanical stretching creates tensile stress that aligns the molecular chains in the direction of the spinning to increase the crystallization of piezoelectric polymers [29,40,48,49]. Such nanofibers have a large surface area to volume ratio, which can be taken advantage of during biomechanical energy conversion, and the fabrication approach also benefits from the use of various electrospinnable materials. Using this method, pristine piezoelectric nanofibers can enhance piezoelectricity without additives, showcasing superior flexibility compared to piezoelectric ceramics, making them pivotal for flexible and wearable electronics. However, despite the straightforward fabrication process, conventional nontextured polymeric nanofibers fail to exhibit a well-rounded performance in critical properties, such as flexibility, piezoelectricity, toughness, and permeability, which should be taken into consideration for the sustained application and optimal utilization in flexible electronics, particularly in biomechanical energy harvesting or healthcare related fields for wearable applications. There have been many reports on improving the material performance or device performance with the piezoelectric polymer P(VDF-TrFE) [22,23,39–55] but very few reported literature on achieving a balanced performance that considers all the key properties mentioned above [56–58].

In tackling such a challenge, our approach involves the development of a textured design for the P(VDF-TrFE) nanofibers, drawing inspiration from two key sources in nature: jute fibers and trees. Inspired by the porous interiors of jute fibers to allow easy water transfer in the plant [59,60], we aim to incorporate similar interior pores within the P(VDF-TrFE) nanofibers to enhance compressibility and breathability [42,43,61], offering potential for emerging flexible and wearable electronics. Exploring not only the interior characteristics but also the surface morphology of the piezoelectric polymeric nanofibers, we took motivation from the rough bark texture of trees. Mirroring the toughness of the tree bark, we integrated a wrinkled surface in the design of the nanofibers, increasing surface area and consequently enhancing toughness of the overall nanofibrous membrane through improved stress absorption. Previous studies have also used bioinspiration to influence the design either in the interior or on the surface of their nanofibers [62–65], but our work uses bioinspiration to shape the design of both the interior structure and the exterior morphology of the nanofibers. By optimizing both the interior and surface morphology of the textured piezoelectric nanofibers, a versatile and high performance of electrical, mechanical, and physical properties was demonstrated when considering the power output, flexibility, stretchability, toughness, and permeability in textured nanofiber-based devices, especially when compared to the performance of nontextured nanofiber-based devices.

Herein, we developed a self-powered, flexible, permeable, tough, and lightweight device that demonstrates a high-level and well-rounded performance by utilizing textured P(VDF-TrFE) nanofibers as the functional material for harvesting biomechanical energy and sensing various biophysiological signals. Inspired by nature, the introduction of the textured structure of the nanofibers resulted in enhanced electrical, mechanical, and physical properties when compared to that of the nontextured nanofibers. Specifically, there was more than two-fold enhancement of electrical generation with the textured nanofiber-based device to demonstrate an improved piezoelectric performance. Furthermore, such a device shows its capability in energy harvesting applications by effectively capturing the biomechanical energy generated by the human body, such as from the motion of the elbow bending. Due to the same transduction mechanism, the nanofibrous sensing device was able to sense minute biophysiological signals when placed on the epidermis to demonstrate its capability in self-powered biophysiological sensing applications, which includes sensing the radial pulse from the wrist and seismocardiogram (SCG) signals from the chest. The sensing data was further used to evaluate a range of other physiological parameters, such as the heart rate and the radial arterial augmentation index. Therefore, the development in materials and fabrication methods, device functionalities, textural morphologies, and overall design strategy culminates in the creation of novel bioinspired textured nanofiber-based devices for energy harvesting and sensing applications.

2. Results and discussion

2.1. Design of the textured nanofibers inspired by nature

The overall schematic of the textured nanofiber-based device, utilized as both a biomechanical energy harvester and biophysiological sensor, is shown in Fig. 1. In our work, the textured nanofibers are defined as exhibiting both interior pores and a wrinkled surface. Such textured structure of the nanofibers draws inspiration from nature. The induced interior porosity is inspired by the porous nature of jute fibers, while the wrinkled surface morphology of the nanofibers is influenced by the rough bark texture of trees. Regarding the porous inspiration, jute fibers are hydrophilic and porous materials that are obtained from the plant genus Corchorus [60,66]. They are considered lignocellulosic fibers, in which their interior porosity helps to easily transfer nutrients and water to the plant's root system. The facile transportation can be attributed to the excellent permeability demonstrated by these natural fibers. As such, we have been inspired by these natural fibers and have induced interior pores to the piezoelectric nanofibers, which has the additional benefit of resulting in increased compressibility of the nanofibers. Furthermore, the surface morphology of the nanofibers is inspired by trees with wrinkled bark. In nature, some trees grow rough and jagged tree bark to form a barrier of protection against outside forces, and it can be observed that they appear "tougher" when compared to trees with smooth bark [67]. The functionality of tree bark in terms of toughness can be attributed to various structural and chemical components, and it is crucial for withstanding mechanical stresses like wind, animal activity, or other external forces. Thus, introducing a wrinkled surface enhances the toughness and expands the surface area of the piezoelectric nanofibers due to the dips and crevices of the uneven surface. Therefore, the design and fabrication of nanofibers with both interior pores and wrinkled surfaces would yield materials characterized by exceptional permeability, enhanced compressibility, increased toughness, and expanded surface area, thereby contributing to a well-balanced performance across electrical, mechanical, and physical properties. Such bioinspired, textured nanofiber-based devices excel in multifunctional applications, such as

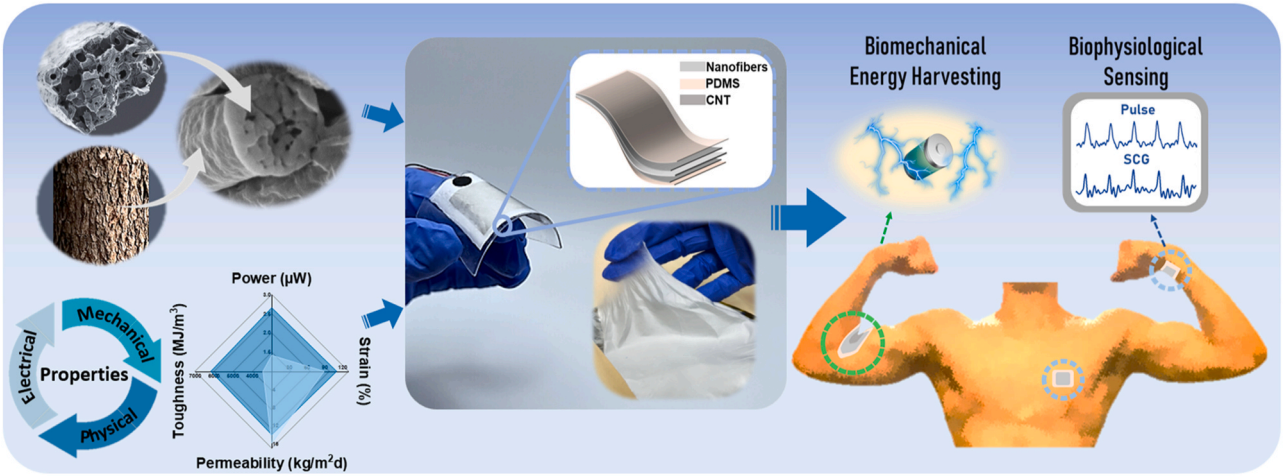

Fig. 1. An overview of the bioinspired, textured, and balanced performance of the P(VDF-TrFE) nanofiber-based device that demonstrates its capability in biomechanical energy harvesting and multifunctional biophysiological sensing applications.

harvesting biomechanical energy and sensing various biophysiological signals for real-time health monitoring (Fig. 1).

2.2. Fabrication and characterization of textured nanofibers

An overview of the fabrication method for the textured nanofibers along with their microscopic structure and chemical properties is illustrated in Fig. 2. Textured P(VDF-TrFE) nanofibers are fabricated mainly based on the vapor-induced phase separation (VIPS) mechanism (Fig. 2a), in which we easily control the relative humidity (RH) of the electrospinning environment (up to 90% RH) at a constant ambient temperature between 65 °F to 70 °F. Previous studies have also obtained porous nanofibers by inducing the VIPS mechanism on other polymers such as polystyrene (PS) and poly(lactic acid) (PLA) [61,68,69], whereas some studies have induced interior pores through the same mechanism onto P(VDF-TrFE) membrane films rather than nanofibers [70,71]. Other studies have introduced interior pores to P(VDF-TrFE) nanofibers using the VIPS mechanism by introducing a controllable humid environment through various methods such as utilizing humidifiers and dehumidifiers inside the electrospinning unit [43,52]. To the best of our knowledge, our work is the first to induce VIPS onto P(VDF-TrFE) nanofibers using a water bath equipment (Fig. 2a) that provides a facile set-up and easily controllable high humidity environment to allow for phase separation of the nanofibers using water vapor to induce interior porosity and wrinkled surface morphologies. This fabrication set-up provides an extremely humid environment with noticeable water vapor condensation on the sides of the equipment while simultaneously allowing for the safe and easy fabrication of porous P(VDF-TrFE) nanofibers. Essentially, when polymer solutions utilize nonvolatile solvents with slow evaporation rates and good water miscibility such as N, N-Dimethylformamide (DMF), water vapor molecules in a high humidity environment have sufficient enough time to penetrate the nanofibers during the solidification process [61]. When volatile solvents with fast evaporation rates such as acetone (ACE) are used, the breath figure (BF) mechanism is induced, in which the volatile solvents evaporate quickly and cause significant temperature drops. As a result, water vapor molecules in a high humidity environment condense on the nanofiber surface to act as placeholders for pores until the water fully evaporates to create a porous surface morphology.

Here, we utilized an equal volume mixture of the ACE and DMF solvents through the electrospinning method that allowed for the incorporation of bioinspired structures in which the ACE:DMF nanofibers solidified and formulated an internal nanoporous structure and a wrinkled surface morphology (see Experimental Section). The VIPS mechanism predominantly determined the fabrication of interior pores to obtain a similar porous morphology as jute fibers, whereas the surface morphology akin to tree bark surfaces was created due to the buckling instability of the polymer jet [43,72]. When a mixture of a volatile and nonvolatile solvent is utilized, the polymer jet forms a glassy skin. As interior pores are formed during the electrospinning process in a high humidity environment, the polymer jet elongates and shrinks, which stretches the glassy skin over the wrinkled formation of the solidifying nanofibers to create uneven surfaces. Since P(VDF-TrFE) is inherently hydrophobic, water acts as a non-solvent for liquid-liquid phase separation to occur [73,74]. In Fig. 2b, the as-spun textured nanofibers can be observed to be lightweight (3 cm × 3 cm, 18 mg) and flexible. The scanning electron microscopy (SEM) images provide the microscopic morphology of the surface and cross-sections of the textured nanofibers respectively in Figs. 2c, d. In Fig. 2c, the SEM image demonstrates excellent alignment of the nanofibers, while the inset shows the wrinkled surface morphology on the aligned P(VDF-TrFE) nanofibers. Interior pores (diameter of approximately 54 nm) can also be observed in the SEM image (Fig. 2d) due to the VIPS mechanism being induced in the high humidity environment. Figs. 2e, f demonstrate the chemical properties of the fabricated textured P(VDF-TrFE) nanofibers, in which the crystalline structure and β-phase fraction were analyzed by X-ray diffraction (XRD) and Fourier transform infrared (FTIR) spectroscopy respectively. In Fig. 2e, the comparison of the diffraction spectrum of the textured and nontextured P(VDF-TrFE) nanofibers is provided, with crystallinities of 83% and 72% respectively. A high crystallinity of 83% is observed for the textured nanofibers due to the mechanical stretching and in situ poling that occurs during the fabrication process of porous nanofibers with wrinkled surfaces in a high humidity environment, whereas the nontextured nanofibers with no pores and smoother surfaces are fabricated in a low humidity environment. Fig. 2f further compares FTIR spectra of textured and nontextured P(VDF-TrFE) nanofibers. The textured nanofibers had β-phase relative fraction percentage of approximately 86%, while the nontextured nanofibers showed around 74%. Here, the β-phase relative fraction was expressed by $F(\beta) = A_\beta / ((K_\beta/K_\alpha)A_\alpha + A_\beta)$, where F(β) is the β-phase relative fraction, K is the absorption coefficient at specified wavenumbers, and A is the absorption band at specified wavenumbers [75,76]. A higher β-phase formation is observed in the textured nanofibers when compared to that of the nontextured nanofibers due to the fabrication of the textured nanofibers in a high humidity environment (up to 90% RH), which lowers the evaporation rate of the solvent [42,43,77]. With a decreased evaporation rate of the ACE:DMF solvent, higher crystallinity can be achieved since the polymer crystallization process is slow and requires sufficient time to align molecular polymer chains during the mechanical stretching process of the nanofibers.

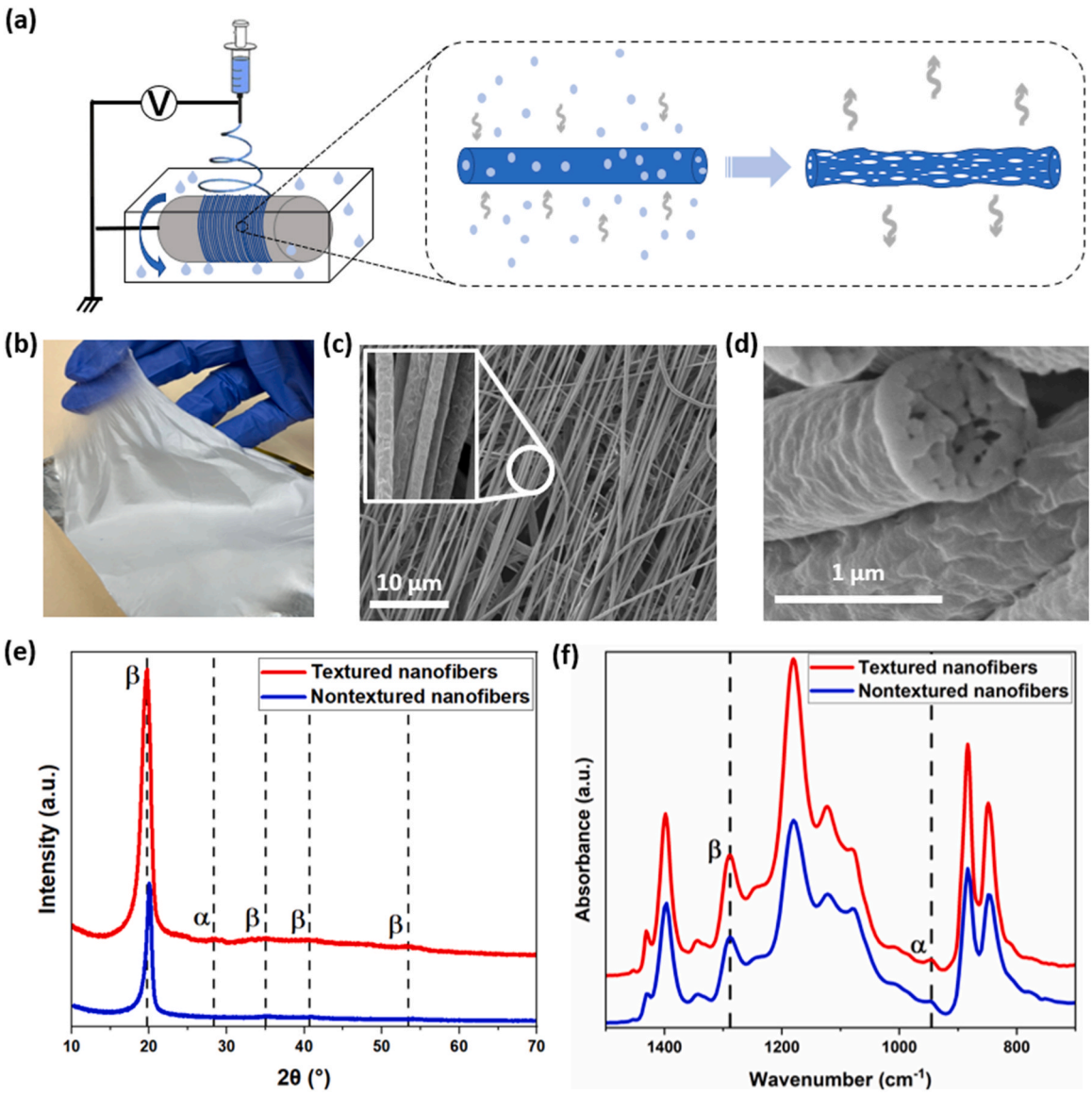

Fig. 2. The working mechanism, microscopic structure, and chemical properties of the textured P(VDF-TrFE) nanofibers. (a) Schematic showing the working mechanism of the induced porosity and wrinkled surface morphology of the nanofibers. (b) Digital image of the electrospun textured nanofibers on the aluminum foil substrate. (c) SEM image of aligned textured nanofibers. Inset shows the wrinkled surface morphology of the textured nanofibers. (d) Cross-sectional SEM image of the textured nanofibers showing interior porosity. (e) XRD comparison of the textured nanofibers and the nontextured nanofibers. (f) FTIR spectra comparison of the textured nanofibers and the nontextured nanofibers.

To study the impact of the inner porous structures and wrinkled surface morphology on the performance of textured P(VDF-TrFE) nanofibers, a systematic evaluation was conducted. Fig. 3 demonstrates the well-balanced performance of the fabricated textured P(VDF-TrFE) nanofibers, with an assessment based on their electrical, mechanical, and physical properties. To design and fabricate the device, the nanofibrous membrane was sandwiched between two encapsulation layers, which are electrode-coated elastomers of polydimethylsiloxane (PDMS) that are flexible and biocompatible [78]. To fabricate an overall flexible device that can harvest biomechanical energy from the human body, compliant electrodes and conformal outer layers are essential since such devices are able to sustain large deformations to maximize the amount of energy harvested. Due to their excellent electrical conductivity and great mechanical strength, single-walled carbon nanotubes (CNTs) were utilized as the electrodes for the energy harvesting device [13,79]. The interplay between the surface adhesion of the PDMS and the conduction induced by the network percolation allowed for contact pressing to easily transfer the patterned CNTs onto the elastomer (see Experimental Section). After fabricating the textured nanofiber-based device, electrical signals are generated after applying pressure due to the piezoelectric effect of the P(VDF-TrFE) nanofibers (see Supporting Information, Figure S1). Essentially, the free dipoles within the piezoelectric nanofibrous membrane are randomly oriented in the presence of no pressure. After applying pressure, the dipoles align themselves in the direction of the applied pressure so that the net dipole moment is no longer zero, in which there is a net positive charge on one electrode layer (i.e., top layer) and a net negative charge on the other electrode layer (i.e., bottom layer). During the application of pressure, the piezoelectric material generates a piezoelectric potential between the two electrodes, thus driving the flow of electrons in one direction. At the fully compressed state, there is no longer any piezoelectric potential, specifically no flow of electrons, since an equilibrium state is achieved. When pressure starts to release, the aligned dipoles will then return to their randomly oriented state, which then results in the flow of electrons in the opposite direction.

To evaluate the electrical properties, a conventional test using a

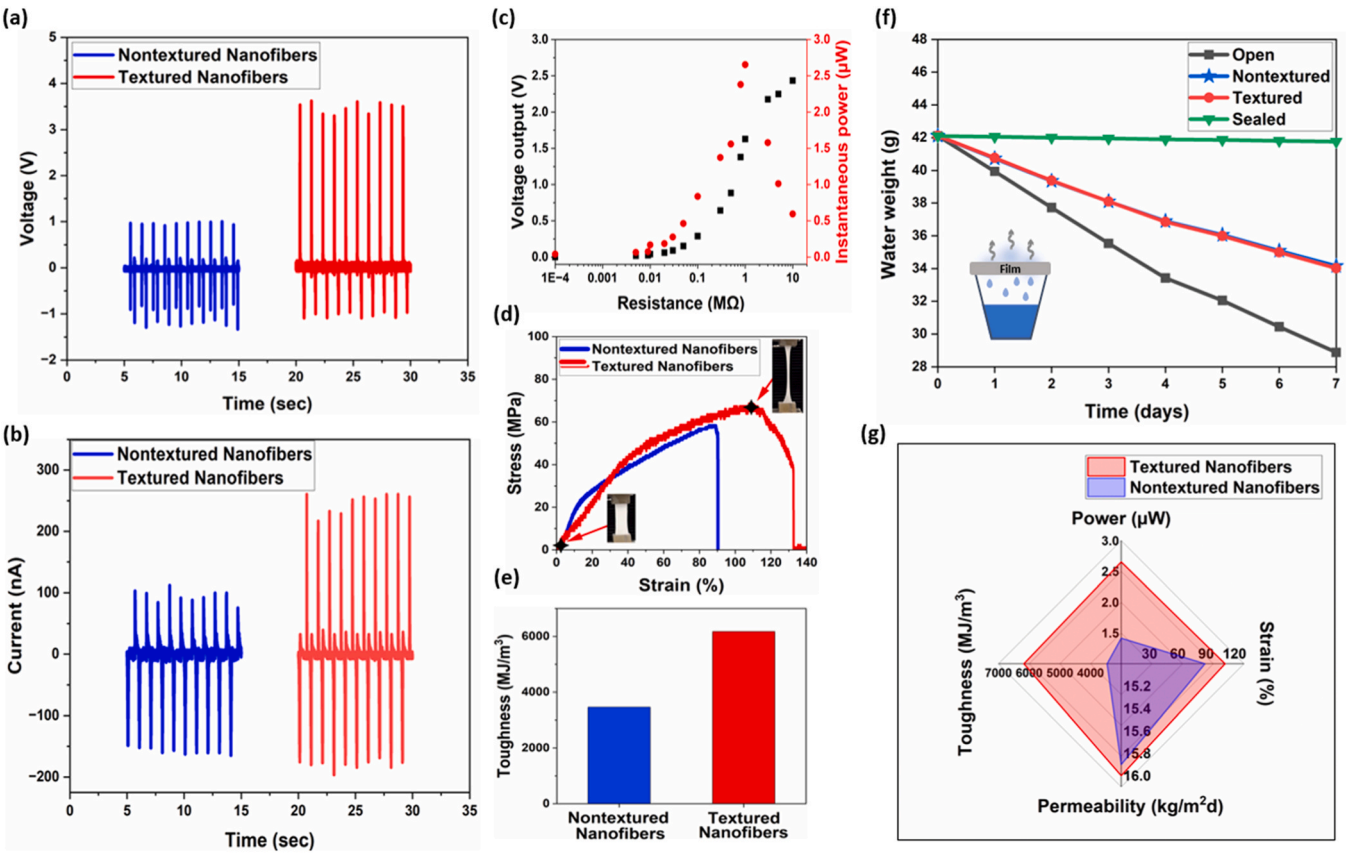

Fig. 3. Balanced performance of the electrical, mechanical, and physical properties of the textured P(VDF-TrFE) nanofibers. (a) Voltage output comparison of the textured and nontextured nanofibrous devices using a 20 N applied normal force at 1 Hz. (b) Current output comparison of the textured and nontextured nanofibrous devices using a 20 N applied normal force at 1 Hz. (c) Output voltage and power at different load resistances using a 20 N applied normal force at 1 Hz. (d) Tensile stress-strain curve comparison of the textured and nontextured P(VDF-TrFE) nanofibers. Left inset shows initial stage of no stretching for the textured nanofibers; right inset shows last stage of stretching before fracture of the textured nanofibers. (e) Toughness comparison of textured and nontextured nanofibers. (f) Water vapor permeability graph demonstrating water vapor loss for four cases: open container, container covered with textured nanofibers, container covered with nontextured nanofibers, and container completely sealed with plastic wrap. (g) Radar graph showing a balanced performance of the electrical, mechanical, and physical properties of the textured nanofibers (red) when compared to the nontextured nanofibers (blue).

shaker-based testing platform was designed to assess the mechanical-to-electrical energy conversion of the piezoelectric material. Briefly, the function generator and shaker provided mechanical excitation to the energy harvesting devices at varying forces and frequencies, and the electrical output signals from the devices were recorded by an oscilloscope. A force sensor was fitted to the loading probe to measure the force magnitude of the mechanical excitation, which was collected using a data acquisition (DAQ) card. An optics set-up was configured to uphold the energy harvesting device at the same height as the shaker's loading probe, which was fitted with a testing head (see Experimental Section). Figs. 3a and b respectively show the voltage and current output generated by both textured-based and nontextured-based energy harvesting devices when subjected to a mechanical input of 20 N and an excitation frequency of 1 Hz. Here, the textured nanofibers were fabricated by using the solvent ACE:DMF and the nontextured using the solvent DMF. In Fig. 3a, it was found that the voltage output produced by the textured nanofibers was significantly higher when compared to that of the nontextured ones, with more than two-fold enhancement of voltage output. Like the voltage output, the current output produced by the textured nanofibers (Fig. 3b) was also higher when compared to that of the nontextured nanofibers, with almost two-fold enhancement. Such nanofibrous texture results in an enhancement of generated voltage and current signals due to two main reasons: the interior pores and the wrinkled surface morphology. Much like jute fibers, there is an increase of compressibility from the interior pores of the P(VDF-TrFE) nanofiber that consequently leads to an increase of deformation. The rough and wrinkled surface morphology also contributes to larger compressibility due to the uneven surfaces that can be compressible. Since the piezoelectric charge coefficient is directly proportional to the compressibility of the overall structure, an improvement of the generated electrical output can be observed (see Supporting Information) [15,80,81]. Furthermore, for nanofibers also demonstrating wrinkled surface morphology, there is higher specific surface area for each individual nanofiber when compared to that of smooth, nontextured nanofibers, which is comparable to trees that are covered with rough bark as opposed to smooth bark [42,43]. As a result, the increased contact areas allow for accumulation of more electrical charges on the surface of the piezoelectric structure, thereby enhancing the piezoelectric output.

Further experimentation was achieved to characterize the electrical performance, XRD, flexibility, and permeability of the textured-based energy harvesting device by tuning solvent ratios of ACE:DMF, the weight percentage of P(VDF-TrFE), and the relative humidity conditions (see Supporting Information, Figures S2-S4). Through conventional testing, it was determined that an equal volume mixture of ACE:DMF at 18 wt% and 90% RH produced the highest voltage generation. In particular, increasing relative humidity of the textured nanofibers from 60% RH to 90% RH increased the levels of porosity (from 1.4% to 8.6%) and pore diameter size (from approximately 24 nm to 54 nm), which directly correlated to an enhancement of electrical output (2.3 V to 4.5 V), whereas the nontextured nanofibers with no interior pores had a voltage output of 2.2 V (see Supporting Information, Figure S4). Such voltage characterization for all samples was supplemented with XRD

analyses, in which the highest observed crystallinity corresponded with the highest voltage output using ACE:DMF at a solvent ratio of (1:1), 18 wt%, and 90% RH. Furthermore, microscopic morphology has also been characterized through SEM using different solvents such as DMF, ACE, and ACE:DMF at different relative humidity conditions (see Supporting Information, Table S1). By changing the relative humidity from 50% (ambient humidity) to 90%, it was found that the dominating porous mechanism was the VIPS mechanism to induce interior porosity for the DMF and ACE:DMF nanofibers. Regardless of the relative humidity, the BF mechanism dominated for the ACE nanofibers to induce surface porosity. To evaluate the power output generated by the textured nanofiber energy harvesters in practice, the electrical outputs were measured by tuning the load resistances ranging from 100 Ω to 10 MΩ, and the instantaneous power was determined accordingly (Fig. 3c). At a resistance of 1 MΩ, the observed maximum voltage output led to an instantaneous power of 2.7 μW by utilizing a variant of Ohm's Law, $P = V^2/R$, in which V is the voltage output and R is the load resistance. Ultimately, textured P(VDF-TrFE) nanofibers with wrinkled surfaces and interior pores demonstrated significantly enhanced electrical properties when compared to that of the nontextured nanofibers.

To evaluate the mechanical properties of the piezoelectric nanofibers, a tensile test was conducted. In Fig. 3d, textured P(VDF-TrFE) nanofibers showed a high stretchability up to a strain of 110% and an elastic modulus of approximately 130 MPa, demonstrating the highly flexible nature of the textured nanofibers, whereas the nontextured nanofibers demonstrated a strain of approximately 89% and an elastic modulus of approximately 230 MPa. The toughness of the nanofibers was determined based on the tensile testing results (Fig. 3**e**), showing that the textured nanofibers exhibited a toughness value of 6173 MJ/m^3, while the nontextured nanofibers had a toughness of 3460 MJ/m^3. Specifically, due to the wrinkled nature of the nanofibrous surface, a deformable physical formation has been obtained for each individual nanofiber. Such wrinkled structures can absorb the applied stress by expanding and smoothing out the wrinkled formation before plastic deformation and fracturing occur [82]. For further testing on mechanical properties, tensile tests were conducted for all nanofibrous samples prepared at different preparation conditions to obtain Young's Modulus values within the 50 to 300 MPa range (see Supporting Information, Figures S2-S4).

Furthermore, the water vapor permeability test was conducted by measuring the amount of water vapor loss through the textured and nontextured nanofibers. The water vapor loss with the nanofibrous membranes was also compared with the water vapor loss of completely open and completely sealed control groups (Fig. 3f, and Experimental Section). Regardless of nanofibrous texture, the water vapor permeability values exhibited similar trends to the completely open case to demonstrate remarkable breathability of nanofibers in general. It was found that the measured permeability value of the textured nanofibers was slightly higher than that of the nontextured nanofibers, with a value of 16.0 $kg\text{-}m^{-2}\cdot d^{-1}$, to indicate improved breathability of the textured nanofibers for wearable electronics. The porosity within the textured nanofibers allowed for the water vapor molecules to easily diffuse throughout the nanofibrous membrane layer to evaporate relatively unimpeded. Ultimately, as shown in Fig. 3g, the instantaneous power, stretchability, permeability, and toughness of the textured P(VDF-TrFE) nanofibers respectively reach 2.7 μW, strain of 110%, 16.0 $kg\text{-}m^{-2}\cdot d^{-1}$, and 6173 MJ/m^3, which are all higher than the value of the nontextured nanofibers and thus demonstrate a balanced and improved performance of the electrical, mechanical, and physical properties of textured fibrous structures. Such enhanced behavior of the properties can be summarily explained by the engineered nanopores through the developed VIPS approach, as well as the wrinkled nature of the nanofibrous surface, which directly leads to an increase of compressibility and expanded surface area that occurs with the textured formation of the P(VDF-TrFE) nanofibers. Permeability tests were also conducted for the nanofibrous samples prepared at different preparation conditions and subsequently tested in different environments, in which the permeability values for the textured nanofibers were calculated to be between approximately 17 to 20 $kg\text{-}m^{-2}\cdot d^{-1}$, while the nontextured nanofibers had the lowest permeability value $^{-1}$ (see Supporting Information, Figures S2-S4).

2.3. Energy harvesting applications

Due to the enhanced electrical properties of textured nanofibers and self-powered feature of piezoelectric materials, such textured nanofiber-based devices make excellent candidates for biomechanical energy harvesting applications. Fig. 4 provides the device characterization as an energy harvesting device fabricated with textured nanofibers, in which the voltage output generation was achieved through conventional tests using the shaker-based platform by tuning forces (Fig. 4a) and excitation frequencies (Fig. 4b). In Fig. 4a, the electrical output at different forces (5 N, 10 N, 15 N, 20 N, and 25 N at a constant frequency of 1 Hz) was measured with the peak-to-peak voltage outputs increasing from 1.3 V to 6.6 V ($R^2 = 0.95658$). Increase of the output voltage with increasing force can be expressed by $V = g_{33} \times F \times t/A$, where V is the electric voltage, g_{33} is the piezoelectric voltage constant, F is the applied force, t is the thickness of the material, and A is the effective area of the specimen [83]. The energy harvesting performance at different excitation frequencies (1 Hz, 1.5 Hz, 2 Hz, 2.5 Hz, 3 Hz, 3.5 Hz, and 4 Hz at a constant input force of 20 N) was further evaluated (Fig. 4b), with the electrical output increasing from 4.5 V to 12.3 V ($R^2 = 0.96502$). Such phenomenon can be further explained by $I = d_{33} \times A \times d\sigma/dt$, in which I is the piezoelectric current, d_{33} is the piezoelectric charge coefficient, A is the effective area of the device, and $d\sigma/dt$ is the mechanical stress changing rate [84]. It has been observed that increasing the mechanical input generally leads to a proportional increase in the output voltage, following a relatively linear relationship [13,83–85].

The measure of durability and stability of energy harvesters is also a significant characteristic to evaluate the devices' long-term performance. The durability of our textured nanofiber-based device was determined through a bending test at over 10,000 cycles. (see Supporting Information, Figure S5). As seen from the insets of Figure S5, the beginning and ending voltage cycles from the bending test show no obvious degradation of the voltage amplitudes despite the harsh mechanical input given to the device over a long period of time. Also, the anti-fatigue results from Fig. 4c show that no significant degradation to the electrical outputs at 10,000 cycles could be observed (mechanical input of 5 N and excitation frequency of 1 Hz). As can be seen from the insets of Fig. 4c, the beginning and ending voltage cycles from the anti-fatigue test demonstrate similar voltage amplitudes. To showcase practical implementation of the energy harvesting device, a full-bridge rectifier was adopted to convert the input alternating current (AC) voltage produced by the piezoelectric material into output direct current (DC) voltage to charge capacitors (Fig. 4d) and light up LEDs (Figs. 4e, f). In Fig. 4d, a charging test was performed by connecting 1 μF, 3.3 μF, and 10 μF capacitors to the device with a rectifying bridge. For the 10 μF capacitor, it took 43 s for the device to reach ~ 0.18 V (input force of 20 N and an excitation frequency of 4 Hz). To demonstrate the practical capabilities of this energy harvester, the device is shown lighting up five green LEDs as a response to hand tapping (Fig. 4**e**, and Supporting Information, Video S1). In addition, the device was also attached to the volunteer's inner elbow. By fully bending the elbow, the device subsequently folded in half due to its inner elbow placement between the forearm and upper arm, and it then harvested enough biomechanical energy to light up a green LED (Fig. 4f, and Supporting Information, Video S2). Those results indicate that the energy harvesting device, which is fabricated based on textured nanofibers, effectively captures and utilizes the biomechanical energy generated through human body movements.

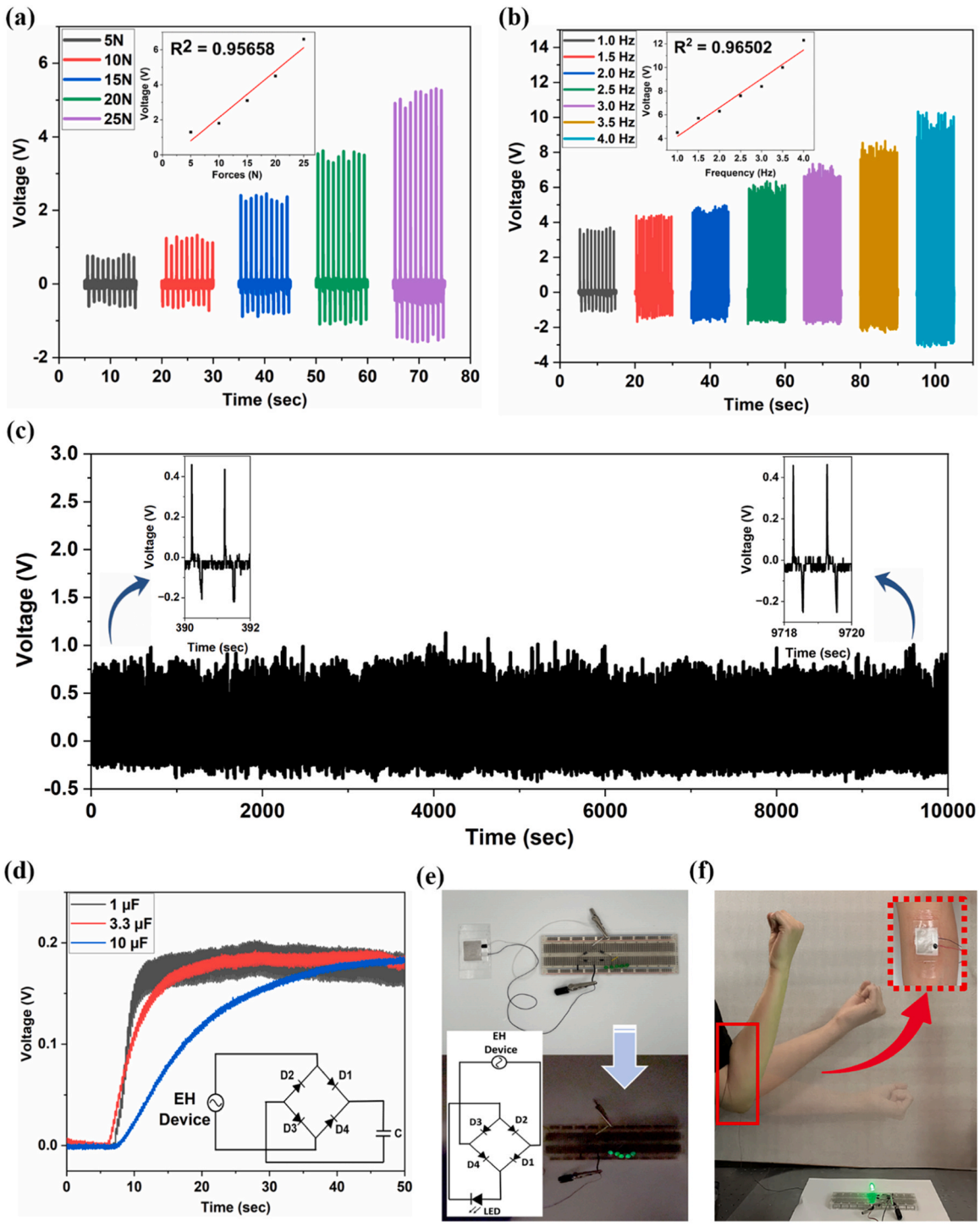

Fig. 4. Device characterization of the energy harvesting device created with textured P(VDF-TrFE) nanofibers. (a) Voltage outputs of the textured nanofiber-based device under difference forces from 5 N to 25 N at a constant excitation frequency of 1 Hz. (b) Voltage outputs of the textured nanofiber-based device under difference excitation frequencies from 1 Hz to 4 Hz at a constant applied force of 20 N. (c) Anti-fatigue testing of the device at a constant force of 5 N at 1 Hz at 10,000 cycles. Left inset shows two cycles of the voltage output at the beginning of the test; right inset shows two cycles of the voltage output towards the end of the test. (d) Measured voltages of various charging capacitors charged by the device at 20 N and 4 Hz. Inset shows the circuit connection with a rectifier to a capacitor. (e) Demonstration of the device's energy-harvesting capabilities by lighting up 5 LEDs in series connection before applying pressure (top) and after applying pressure (bottom). Inset shows the circuit connection with a rectifier to LEDs. (f) Demonstration of the device's biomechanical energy-harvesting capabilities by lighting up an LED through the mechanical motion of the elbow bending.

2.4. Biophysiological Sensing Performance

In addition to energy harvesting applications, the same textured nanofiber-based device can be used in multifunctional sensing applications due to the same piezoelectric effect, where the presence of external pressure (such as the radial pulse or surface vibrations caused by the arm muscle contractions) allows the polarized dipoles within the piezoelectric material to orient themselves such that the net positive and net negative charges are distributed on opposite surfaces of the functional material [15]. This creates a piezoelectric potential, which causes

electrons to flow out to a connected circuit. Especially due to its conformity to the human skin, the fabricated textured nanofibrous sensor was favorable for biophysiological sensing applications, such as blood pressure sensing, mechanomyography (MMG) sensing, and SCG sensing [86]. As shown in Fig. 5a, the device was attached to the wrist for pulse sensing. The real-time voltage signals generated from the textured nanofiber-based device were measured (see Supporting Information, Video S3), approximating the pulse rate as 80 beats per minute (BPM) (Fig. 5b). This calculation is consistent with the readings obtained from a commercial blood pressure monitor, which provided a pulse rate of 78 BPM (Fig. 5b, right inset). The left inset shows one pulse waveform, in which two definitive signal peaks (P_1 and P_2) can be clearly observed. Within a single radial artery pressure wave, P_1 represents the sum of the ejected incident wave and the reflected wave from the hand, while P_2 represents the reflected wave peak from the lower body without the inclusion of the end-diastolic pressure [87]. With these two distinct peaks, the radial arterial augmentation index (AI_r) can be determined to measure the level of systemic arterial stiffness. By using $AI_r = P_2/P_1$ to calculate the arterial stiffness, the 29-year-old volunteer had an AI_r of approximately 0.52, which was considered to be within the normal range of a healthy person in his or her 20 s [87]. We also collected another volunteer's pulse data from the wrist (see Supporting Information, Figure S6). The sensor was able to measure similar real-time voltage signals, with an approximate pulse rate of 78 BPM, whereas the commercial blood pressure monitor provided a pulse rate of 76 BPM. Moreover, the second volunteer's AI_r value was computed at approximately 0.41, which was also considered to be within the normal range of a healthy person in his or her 20 s [87].

The MMG sensing performance of the textured nanofiber-based sensor was further demonstrated by attaching the sensor to the outer forearm (Fig. 5c). For this sensing, the muscle mechanical activity of the forearm muscle, or more specifically the flexor digitorum profundus, is

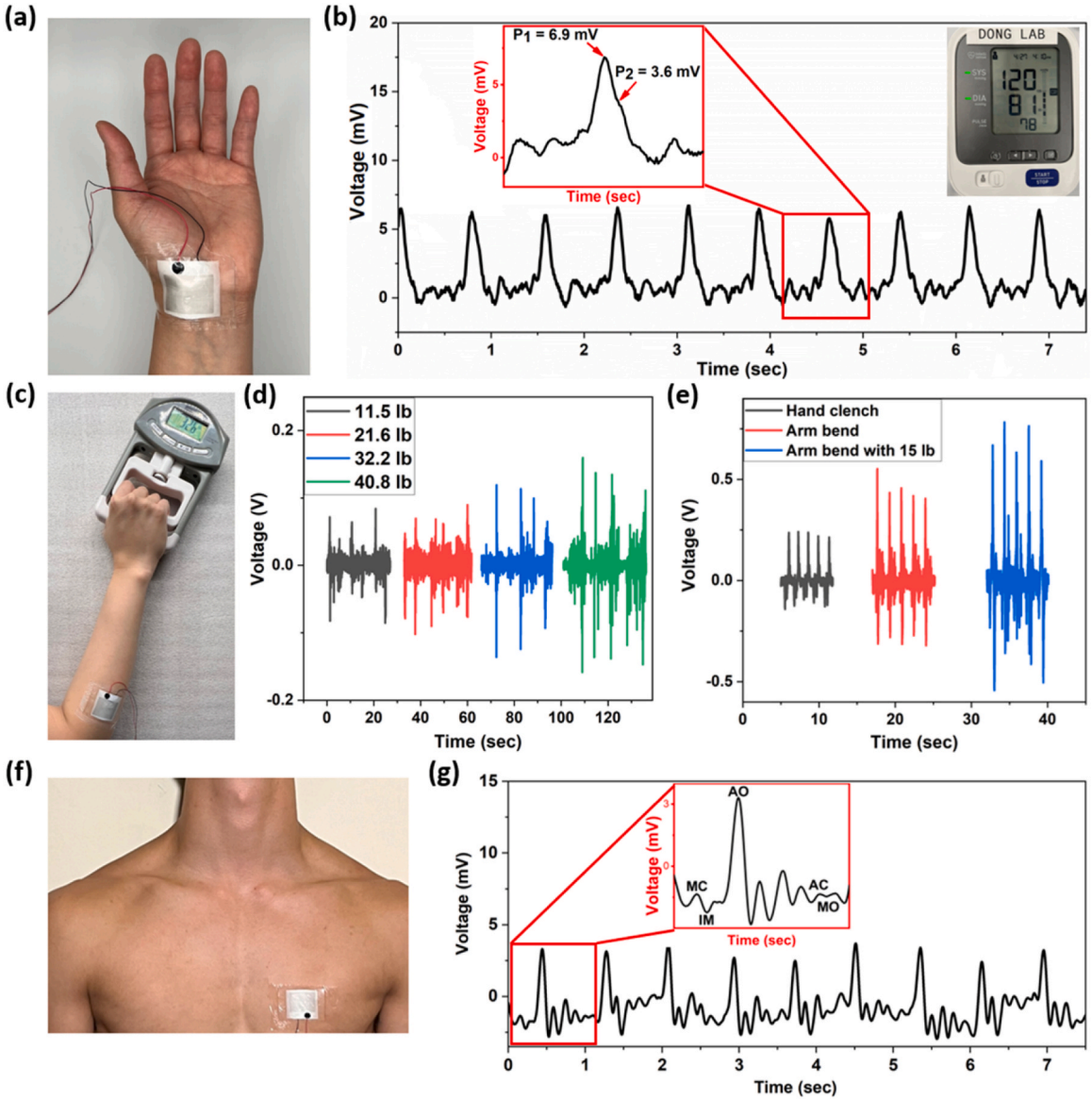

Fig. 5. Biophysiological sensing applications using the textured P(VDF-TrFE) nanofibers. (a) Digital image of the device attached to the upper wrist area for pulse detection. (b) Voltage signals of the sensor attached to the upper wrist. The left inset shows a single pulse waveform with two peaks annotated while the right inset shows the blood pressure and pulse rate values from a commercial blood pressure monitor. (c) Digital image of the device attached to the forearm while the volunteer is holding onto a gripper. (d) Voltage signals of the sensor attached to the forearm while the volunteer used the gripper at various loads. (e) Voltage signals of the sensor attached to the forearm while the volunteer does various exercises. (f) Digital image of the device attached to the chest for SCG sensing. (g) Voltage signals of the sensor attached to the chest. The inset shows a single SCG waveform with important peaks annotated.

observed through grip force testing (Fig. 5d) and various arm exercises (Fig. 5e). As the muscle goes through contractions, the shape of the muscle is deformed in some manner, which subsequently causes vibrations of the muscle fibers [86]. The vibrations cause external pressure to be applied to the piezoelectric sensor, which then detects the resultant piezoelectric potential [15]. As shown in Fig. 5d, various grip loads were tested (averaging 11.5 lb, 21.6 lb, 32.2 lb, and 40.8 lb), which provided increasing electrical outputs. As the hand clasped the gripper with increasing loads, it caused the forearm muscle to contract more, thus creating higher voltage amplitudes of MMG signals, especially for the 40.8 lb load since the trembling of the arm could be visually observed during testing. Additionally, various arm motion activities were tested using the same position of the sensor on the forearm, in which the volunteer did hand clenching, arm bending, and arm bending while holding a 15 lb weight (Fig. 5e). The hand clenching generated MMG signals with the smallest amplitudes due to the minimum contraction of the forearm's profundus muscle during the motion of the hand, and the arm exercise with the 15 lb weight generated MMG signals with the largest amplitudes since the profundus muscle contracted more with additional weight. By holding a weight, the mechanical activity of the forearm muscle increases as the muscle deforms to a greater extent when compared to the amount of muscle deformation for arm bending without a weight, which corresponds to higher amplitudes of the MMG signals. Additional sensing applications were demonstrated by placing the textured nanofiber-based sensor on the center of the wrist. The wrist was then flexed upwards and extended downwards, and the sensor was able to sense MMG signals of the wrist motion (see Supporting Information, Figures S7-S8).

To demonstrate the versatility of the textured nanofiber-based sensor for biophysiological sensing applications, the sensor was attached to a male volunteer's chest, specifically positioned at the mitral valve to detect SCG signals (Fig. 5f). SCG is a non-invasive method of measuring the heart's mechanical activity by detecting the vibrations of the thorax wall. The peaks observed in SCG correspond to various physiological cardiac events [12,88–90]. In Fig. 5g, the sensing signals of the voltage output generated from the textured nanofibrous sensor were measured, revealing an SCG waveform with annotated peaks. The first set of peaks correspond to systolic activities, including the mitral valve closure (MC), isovolumic moment (IM), and the aortic valve opening (AO); the second set of peaks correspond to diastolic activities, which include the aortic closure (AC) and mitral valve opening (MO) [90]. Understanding these significant maximum and minimum points of SCG waves is crucial. Any detected irregularities in the waveform's structure can immediately alert healthcare professionals to potential cardiac-related issues. For example, low amplitudes of SCG points such as point AO can correlate to a reduced coronary blood flow, which could indicate cardiac diseases such as coronary artery stenosis or ischemia [12,91]. Moreover, by measuring the distance between point AO and other SCG peak points and comparing the normal time interval of healthy subjects with that of unhealthy subjects, it could suggest other cardiac-related diseases and conditions such as arrhythmia or myocardial ischemia and could aid in preemptive measures to prevent detrimental cardiac events [92]. With the piezoelectric effect as the transduction mechanism of the material, the device using textured P(VDF-TrFE) nanofibers was capable of harvesting biomechanical energy and self-powered sensing of biophysiological signals from the human body.

3. Conclusions

We have developed self-powered, flexible, permeable, tough, and lightweight energy harvesting and sensing devices using textured P(VDF-TrFE) nanofibers for wearable electronics applications. Our multifunctional device can attach conformably to the human skin to effectively energy harvest from the biomechanical motions of the human body and to continuously sense real-time biophysiological signals. Through the integration of the VIPS mechanism and a facile electrospinning technique, we have introduced both interior porous structures and a wrinkled surface morphology to design textured nanofibers that derive bioinspiration from jute fibers and tree bark respectively. Those engineered textured structures of the nanofibers enhance compressibility and expand surface area of the polymeric fibrous membrane, and thus improve the device's electrical performance by more than two-fold when compared to that of the nontextured P(VDF-TrFE) nanofiber device. Along with the electrical properties, the mechanical and physical properties have also been improved due to the enhanced toughness and permeability of the textured nanofibers, resulting in an overall well-rounded performance. The flexible and wearable device, employing textured P(VDF-TrFE) nanofibers as the functional material, demonstrates its capability as a biomechanical energy harvester by illuminating an LED using the motion of the elbow. Furthermore, such textured nanofiber-based devices also serve as a non-invasive health monitoring solution by sensing various biophysiological signals, such as pulse wave, MMG, and SCG, and they enable quick and efficient health analysis through real-time monitoring. By demonstrating a balanced and enhanced performance, this novel design strategy of textured P(VDF-TrFE) nanofibers facilitates the advancement of wearable bioelectronics for the next generation of flexible electronics utilized in multifunctional applications.

4. Experimental section

4.1. Preparation of textured P(VDF-TrFE) nanofiber device

P(VDF-TrFE) solution: The solvent mixture was prepared by combining an equal volume ratio (1:1) of N,N-Dimethylformamide (Sigma-Aldrich) and Acetone (Sigma-Aldrich). Then, the P(VDF-TrFE) solution was prepared by dissolving 18 wt% P(VDF-TrFE) powder (70/30 mol; Arkema) to the solvent under magnetic stirring conditions for over 6 h at 60 °C.

Fabrication of textured nanofibers: The electrospinning unit (MTI Corporation) was used to electrospin the P(VDF-TrFE) nanofibers. The water bath equipment (Fisherbrand) was placed inside the electrospinning unit, filled with deionized (DI) water, and set at a temperature range of 25 to 50 °C to get the desired relative humidity. One humidity sensor was placed inside the water bath, and another was placed outside the water bath to monitor the electrospinning environment humidity. Parameters for the electrospinning unit were initially set to 18 kV (applied voltage), 12 cm (distance to collector), 2000 rpm (mandrel rotating speed), 1 mL/hr (feed rate), and 1 hr (time). The nanofibers were then annealed at 135 °C for 2 hr.

Encapsulation layers: Silicone elastomer base (Dow Chemical Company, Sylgard 184) was mixed with the curing agent at a ratio of 10:1 to prepare the PDMS solution. A vacuum spin coater (MTI Corporation) was used to spin coat the PDMS solution onto a glass slide at 500 rpm for 30 s. Then it was partially cured in the oven at 60 °C for 30 min. Meanwhile, the CNT solution was prepared by ultrasonicating the CNT solution and vacuum filtrating onto a polytetrafluoroethylene (PTFE) membrane filter (pore diameter of 47 nm) to create a CNT percolating mat. Finally, CNT was transferred to the partially cured PDMS substrate by contact pressing. A specific pattern of the CNT was formed onto the PDMS substrate using a Mylar film mask.

Device assembly: The multilayer device was assembled by preparing the active electrospun textured P(VDF-TrFE) fibrous membrane and two encapsulation layers. Two electrical wires were attached to the encapsulation layers, and then, the textured nanofiber layer was sandwiched between the two encapsulation layers. The overall device dimensions measured 4.8 cm × 3.5 cm while the active P(VDF-TrFE) fibrous membrane measured 3.3 cm × 3.3 cm, which was slightly larger than the testing head (2.5 cm × 2.2 cm) affixed to the shaker's loading probe in which it made contact with the active layer during conventional tests.

4.2. Characterization methods

The microscopic morphology (surface, alignment, and cross-section) of the textured nanofibers was observed through SEM (JEOL JSM-9700 F). To obtain the cross-section of the nanofibers, the freeze fracturing technique in liquid nitrogen was used. The phase identification was measured through XRD (PANalytical Empyrean) and FTIR (Agilent Cary 670). The tensile experiments were measured using a motorized tension test stand (MARK-10). The testing area of the textured nanofiber sample was measured at 8 mm × 20 mm with a thickness of 20 μm, and the speed of the tensile test was set at 30 mm/min. The gas permeability experiment was conducted by using containers filled with DI water. The experiment had two control groups (opening left uncovered; opening fully sealed with plastic wrap) and two test groups (opening fully covered with textured and nontextured P(VDF-TrFE) nanofibers). The containers were placed inside a chamber with a constant relative humidity (20–30 RH%), and the permeability was calculated by measuring the DI water weight loss every 24 h for 7 days.

4.3. Testing set-up

A shaker-based platform was designed and built for conventional test experiments. A function generator (Keysight) was connected to a power amplifier (The Modal Shop), which then supplied the input excitation to the shaker (The Modal Shop). The shaker provided the mechanical input to the device, which was firmly affixed to a fixture frame (Newport). The real-time electrical output generated by the device was collected and measured by a voltage pre-amplifier (Stanford) and an oscilloscope (Keysight DSOX1204A). For current measurements, a current pre-amplifier (Stanford) was used. The applied forces were separately measured by a load cell (PCB Piezoelectronics), in which a DAQ card system (National Instruments) collected the data through the LabView software. The experiments involving human subjects have been performed with the full, informed consent of the volunteers, who are also authors of the manuscript.

CRediT authorship contribution statement

Dong Lin: Writing – review & editing, Supervision, Funding acquisition, Conceptualization. **Kwon Sun Hwa:** Writing – original draft, Validation, Formal analysis. **Zhang Chi:** Validation. **Jiang Zhipeng:** Validation, Conceptualization.

Declaration of Competing Interest

The authors declare that they have no known competing financial interests or personal relationships that could have appeared to influence the work reported in this paper.

Data availability

Data will be made available on request.

Acknowledgment

The authors acknowledge financial support from the National Science Foundation award (ECCS 2106459, PI: L.D.), the American Heart Association Institutional Research Enhancement Award (23AIREA1048411, PI: L.D.), and the Startup Fund from the Department of Mechanical and Industrial Engineering at New Jersey Institute of Technology (NJIT).

Appendix A. Supporting information

Supplementary data associated with this article can be found in the online version at doi:10.1016/j.nanoen.2024.109334.

References

[1] S. Mukherjee, A. Albertengo, T. Djenizian, Beyond flexible-Li-ion battery systems for soft electronics, Energy Storage Mater. 42 (2021) 773–785, https://doi.org/10.1016/j.ensm.2021.08.020.
[2] W. Gao, H. Ota, D. Kiriya, K. Takei, A. Javey, Flexible electronics toward wearable sensing, Acc. Chem. Res. 52 (3) (2019) 523–533, https://doi.org/10.1021/acs.accounts.8b00500.
[3] Z. Wang, Y. Cong, J. Fu, Stretchable and tough conductive hydrogels for flexible pressure and strain sensors, J. Mater. Chem. B 8 (16) (2020) 3437–3459, https://doi.org/10.1039/C9TB02570G.
[4] Y. Liu, T. Yang, Y. Zhang, G. Qu, S. Wei, Z. Liu, T. Kong, Ultrastretchable and wireless bioelectronics based on all-hydrogel microfluidics, Adv. Mater. 31 (39) (2019) 1902783, https://doi.org/10.1002/adma.201902783.
[5] Y.J. Hong, H. Jeong, K.W. Cho, N. Lu, D.-H. Kim, Wearable and implantable devices for cardiovascular healthcare: from monitoring to therapy based on flexible and stretchable electronics, Adv. Funct. Mater. 29 (19) (2019) 1808247, https://doi.org/10.1002/adfm.201808247.
[6] E. McAdams, A. Krupaviciute, C. Gehin, A. Dittmar, G. Delhomme, P. Rubel, J. Fayn, and J. McLaughlin, Wearable Electronic Systems: Applications to Medical Diagnostics/Monitoring, in Wearable Monitoring Systems, A. Bonfiglio and D. De Rossi Eds. Boston, MA: Springer US, 2011, pp. 179–203.
[7] L. Kong, C. Tang, H.-J. Peng, J.-Q. Huang, Q. Zhang, Advanced energy materials for flexible batteries in energy storage: a review, SmartMat 1 (1) (2020) 1–35, https://doi.org/10.1002/smm2.1007.
[8] T. Ghomian, S. Mehraeen, Survey of energy scavenging for wearable and implantable devices, Energy 178 (2019) 33–49, https://doi.org/10.1016/j.energy.2019.04.088.
[9] R. Riemer, A. Shapiro, Biomechanical energy harvesting from human motion: theory, state of the art, design guidelines, and future directions, J. Neuroeng. Rehabil. 8 (2011) 1–13, https://doi.org/10.1186/1743-0003-8-22.
[10] Y. Zou, L. Bo, Z. Li, Recent progress in human body energy harvesting for smart bioelectronic system, Fundam. Res. 1 (3) (2021) 364–382, https://doi.org/10.1016/j.fmre.2021.05.002.
[11] L. Dong, A.B. Closson, C. Jin, I. Trase, Z. Chen, J.X.J. Zhang, Vibration-energy-harvesting system: transduction mechanisms, frequency tuning techniques, and biomechanical applications, Adv. Mater. Technol. 4 (10) (2019) 1900177, https://doi.org/10.1002/admt.201900177.
[12] S.H. Kwon, L. Dong, Flexible sensors and machine learning for heart monitoring, Nano Energy 102 (2022) 107632, https://doi.org/10.1016/j.nanoen.2022.107632.
[13] C. Jin, L. Dong, Z. Xu, A. Closson, A. Cabe, A. Gruslova, S. Jenney, D. Escobedo, J. Elliott, M. Zhang, N. Hao, Z. Chen, M.D. Feldman, J.X.J. Zhang, Skin-like elastomer embedded zinc oxide nanoarrays for biomechanical energy harvesting, Adv. Mater. Interfaces 8 (10) (2021) 2100094, https://doi.org/10.1002/admi.202100094.
[14] L. Wang, Z. Fei, Y. Qi, C. Zhang, L. Zhao, Z. Jiang, R. Maeda, Overview of human kinetic energy harvesting and application, ACS Appl. Energy Mater. 5 (6) (2022) 7091–7114, https://doi.org/10.1021/acsaem.2c00703.
[15] J. Curie, P. Curie, Développement par compression de l'électricité polaire dans les cristaux hémièdres à faces inclinées, Bull. De. minéralogie 3 (4) (1880) 90–93.
[16] M.G. Broadhurst, G.T. Davis, J.E. McKinney, R.E. Collins, Piezoelectricity and pyroelectricity in polyvinylidene fluoride - a model, J. Appl. Phys. 49 (10) (1978) 4992–4997, https://doi.org/10.1063/1.324445.
[17] K.K. Sappati, S. Bhadra, Piezoelectric polymer and paper substrates: a review, Sensors 18 (11) (2018) 3605, https://doi.org/10.3390/s18113605.
[18] K.S. Ramadan, D. Sameoto, S. Evoy, A review of piezoelectric polymers as functional materials for electromechanical transducers, Smart Mater. Struct. 23 (3) (2014) 033001, https://doi.org/10.1088/0964-1726/23/3/033001.
[19] L. Dong, C. Jin, A.B. Closson, I. Trase, H.C. Richards, Z. Chen, J.X.J. Zhang, Cardiac energy harvesting and sensing based on piezoelectric and triboelectric designs, Nano Energy 76 (2020) 105076, https://doi.org/10.1016/j.nanoen.2020.105076.
[20] L. Dong, A.B. Closson, M. Oglesby, D. Escobedo, X. Han, Y. Nie, S. Huang, M. D. Feldman, Z. Chen, J.X.J. Zhang, In vivo cardiac power generation enabled by an integrated helical piezoelectric pacemaker lead, Nano Energy 66 (2019) 104085, https://doi.org/10.1016/j.nanoen.2019.104085.
[21] C. Ribeiro, C.M. Costa, D.M. Correia, J. Nunes-Pereira, J. Oliveira, P. Martins, R. Gonçalves, V.F. Cardoso, S. Lanceros-Méndez, Electroactive poly(vinylidene fluoride)-based structures for advanced applications, Nat. Protoc. 13 (4) (2018) 681–704, https://doi.org/10.1038/nprot.2017.157.
[22] S. Mohammadpourfazeli, S. Arash, A. Ansari, S. Yang, K. Mallick, R. Bagherzadeh, Future prospects and recent developments of polyvinylidene fluoride (PVDF) piezoelectric polymer; fabrication methods, structure, and electro-mechanical properties, RSC Adv. 13 (1) (2023) 370–387, https://doi.org/10.1039/D2RA06774A.
[23] X. Chen, H. Li, Z. Xu, L. Lu, Z. Pan, Y. Mao, Electrospun nanofiber-based bioinspired artificial skins for healthcare monitoring and human-machine interaction, Biomimetics 8 (2) (2023), https://doi.org/10.3390/biomimetics8020223.
[24] M.S. Islam, B.C. Ang, A. Andriyana, A.M. Afifi, A review on fabrication of nanofibers via electrospinning and their applications, SN Appl. Sci. 1 (10) (2019) 1248, https://doi.org/10.1007/s42452-019-1288-4.
[25] K. Halicka, J. Cabaj, Electrospun nanofibers for sensing and biosensing applications—a review, Int. J. Mol. Sci. 22 (12) (2021) 6357, https://doi.org/10.3390/ijms22126357.

[26] P. Yao, B. Zhu, H. Zhai, X. Liao, Y. Zhu, W. Xu, Q. Cheng, C. Jayyosi, Z. Li, J. Zhu, K.M. Myers, X. Chen, Y. Yang, PVDF/palygorskite nanowire composite electrolyte for 4 V rechargeable lithium batteries with high energy density, Nano Lett. 18 (10) (2018) 6113–6120, https://doi.org/10.1021/acs.nanolett.8b01421.

[27] H. Soleymani, M. Noormohammadi, M.A. Kashi, M.H. Amiri, J.J. Michels, K. Asadi, M.M. Abolhasani, Self-poled sausage-like pvdf nanowires produced by confined phase inversion as novel piezoelectric nanogenerators, Adv. Mater. Interfaces 8 (5) (2021) 2001734, https://doi.org/10.1002/admi.202001734.

[28] X. Li, Y.-F. Lim, K. Yao, F.E.H. Tay, K.H. Seah, Ferroelectric poly(vinylidene fluoride) homopolymer nanotubes derived from solution in anodic alumina membrane template, Chem. Mater. 25 (4) (2013) 524–529, https://doi.org/10.1021/cm3028466.

[29] M. Steinhart, S. Senz, R.B. Wehrspohn, U. Gösele, J.H. Wendorff, Curvature-directed crystallization of poly(vinylidene difluoride) in nanotube walls, Macromolecules 36 (10) (2003) 3646–3651, https://doi.org/10.1021/ma0260039.

[30] X. Dai, P. Guo, Z. Xing, W. Yang, K. Wang, C. Zhang, X. Chen, Crystallization and melting behavior of polyvinylidene fluoride in confined space of nanotubes, J. Phys.: Conf. Ser. 1986 (1) (2021) 012009, https://doi.org/10.1088/1742-6596/1986/1/012009.

[31] C. Sun, J. Shi, D.J. Bayerl, X. Wang, PVDF microbelts for harvesting energy from respiration, Energy Environ. Sci. 4 (11) (2011) 4508–4512, https://doi.org/10.1039/C1EE02241E.

[32] L. Dong, X. Han, Z. Xu, A.B. Closson, Y. Liu, C. Wen, X. Liu, G.P. Escobar, M. Oglesby, M. Feldman, Z. Chen, J.X.J. Zhang, Flexible porous piezoelectric cantilever on a pacemaker lead for compact energy harvesting, Adv. Mater. Technol. 4 (1) (2019) 1800148, https://doi.org/10.1002/admt.201800148.

[33] K. Sandhu, S. Singh, and C. Mustansar Hussain, 7 - 3D printing of nanomaterials using inkjet printing, in Additive Manufacturing with Functionalized Nanomaterials, S. Singh and C. M. Hussain Eds.: Elsevier, 2021, pp. 155–192.

[34] N. Chen, L. Hong, Surface phase morphology and composition of the casting films of PVDF–PVP blend, Polymer 43 (4) (2002) 1429–1436, https://doi.org/10.1016/S0032-3861(01)00671-1.

[35] M.M. Hasan, M.S.B. Sadeque, I. Albasar, H. Pecenek, F.K. Dokan, M.S. Onses, M. Ordu, Scalable fabrication of mxene-pvdf nanocomposite triboelectric fibers via thermal drawing, Small 19 (6) (2023) 2206107, https://doi.org/10.1002/smll.202206107.

[36] S. Bodkhe, G. Turcot, F.P. Gosselin, D. Therriault, One-step solvent evaporation-assisted 3D printing of piezoelectric PVDF nanocomposite structures, ACS Appl. Mater. Interfaces 9 (24) (2017) 20833–20842, https://doi.org/10.1021/acsami.7b04095.

[37] L. Dong, C. Wen, Y. Liu, Z. Xu, A.B. Closson, X. Han, G.P. Escobar, M. Oglesby, M. Feldman, Z. Chen, J.X.J. Zhang, Piezoelectric buckled beam array on a pacemaker lead for energy harvesting, Adv. Mater. Technol. 4 (1) (2019) 1800335, https://doi.org/10.1002/admt.201800335.

[38] J. Xue, T. Wu, Y. Dai, Y. Xia, Electrospinning and electrospun nanofibers: methods, materials, and applications, Chem. Rev. 119 (8) (2019) 5298–5415, https://doi.org/10.1021/acs.chemrev.8b00593.

[39] G. Kalimuldina, N. Turdakyn, I. Abay, A. Medeubayev, A. Nurpeissova, D. Adair, Z. Bakenov, A review of piezoelectric PVDF film by electrospinning and its applications, Sensors 20 (18) (2020) 5214, https://doi.org/10.3390/s20185214.

[40] Z. He, F. Rault, A. Vishwakarma, E. Mohsenzadeh, F. Salaün, High-aligned PVDF nanofibers with a high electroactive phase prepared by systematically optimizing the solution property and process parameters of electrospinning, Coatings 12 (9) (2022) 1310, https://doi.org/10.3390/coatings12091310.

[41] X. Chen, C. Tougne, T. Jiang, M. Espindola-Rodriguez, Q. Zhao, Q. Jia, H. Mendil-Jakani, J. Jiang, W. Zhang, Highly oriented PVDF molecular chains for enhanced material performance, Polymer 261 (2022) 125366, https://doi.org/10.1016/j.polymer.2022.125366.

[42] B. Zaarour, L. Zhu, X. Jin, A review on the secondary surface morphology of electrospun nanofibers: formation mechanisms, characterizations, and applications, ChemistrySelect 5 (4) (2020) 1335–1348, https://doi.org/10.1002/slct.201903981.

[43] B. Zaarour, L. Zhu, C. Huang, X. Jin, Controlling the secondary surface morphology of electrospun PVDF nanofibers by regulating the solvent and relative humidity, Nanoscale Res. Lett. 13 (1) (2018) 285, https://doi.org/10.1186/s11671-018-2705-0.

[44] M. Kim, S. Lee, and Y.-I. Kim, Solvent-controlled crystalline beta-phase formation in electrospun P(VDF-TrFE) fibers for enhanced piezoelectric energy harvesting, APL Materials, vol. 8, no. 7, p. 071109, 2020, doi: 10.1063/5.0011686.

[45] C. Chen, T. Zhang, C. Zhang, Y. Feng, Y. Zhang, Y. Zhang, Q. Chi, X. Wang, Q. Lei, Improved energy storage performance of P(VDF-TrFE-CFE) multilayer films by utilizing inorganic functional layers, ACS Appl. Energy Mater. 4 (10) (2021) 11726–11734, https://doi.org/10.1021/acsaem.1c02471.

[46] M. Chung, F.J. Diaz Sanchez, J. Schoeller, R. Stämpfli, R.M. Rossi, N. Radacsi, Enhanced piezoelectric performance of electrospun PVDF-TrFE by polydopamine-assisted attachment of ZnO nanowires for impact force sensing, Macromol. Mater. Eng. 308 (6) (2023) 2200520, https://doi.org/10.1002/mame.202200520.

[47] H. Abdolmaleki, A.B. Haugen, K.B. Buhl, K. Daasbjerg, S. Agarwala, Interfacial Engineering of PVDF-TrFE toward higher piezoelectric, ferroelectric, and dielectric performance for sensing and energy harvesting applications, Adv. Sci. 10 (6) (2023) 2205942, https://doi.org/10.1002/advs.202205942.

[48] B. Mahanty, S.K. Ghosh, G. Prasad, A. Shanmugasundaram, D.-W. Lee, Giant energy harvesting via maxwell displacement current enhancement using metal sheet interspaced hetero-layer structured piezo-composite nanofiber device, Adv. Funct. Mater. (2023) 2307723, https://doi.org/10.1002/adfm.202307723.

[49] Z. Shao, X. Zhang, Z. Song, J. Liu, X. Liu, C. Zhang, Simulation guided coaxial electrospinning of polyvinylidene fluoride hollow fibers with tailored piezoelectric performance, Small (2023) 2303285, https://doi.org/10.1002/smll.202303285.

[50] F. Mokhtari, M. Shamshirsaz, M. Latifi, Investigation of β phase formation in piezoelectric response of electrospun polyvinylidene fluoride nanofibers: LiCl additive and increasing fibers tension, Polym. Eng. Sci. 56 (1) (2016) 61–70, https://doi.org/10.1002/pen.24192.

[51] B.S. Athira, A. George, K. Vaishna Priya, U.S. Hareesh, E.B. Gowd, K.P. Surendran, A. Chandran, High-performance flexible piezoelectric nanogenerator based on electrospun PVDF-BaTiO3 nanofibers for self-powered vibration sensing applications, ACS Appl. Mater. Interfaces 14 (39) (2022) 44239–44250, https://doi.org/10.1021/acsami.2c07911.

[52] B. Zaarour, L. Zhu, C. Huang, X. Jin, Enhanced piezoelectric properties of randomly oriented and aligned electrospun PVDF fibers by regulating the surface morphology, J. Appl. Polym. Sci. 136 (6) (2019) 47049, https://doi.org/10.1002/app.47049.

[53] S. Zhang, B. Zhang, J. Zhang, K. Ren, Enhanced piezoelectric performance of various electrospun PVDF nanofibers and related self-powered device applications, ACS Appl. Mater. Interfaces 13 (27) (2021) 32242–32250, https://doi.org/10.1021/acsami.1c07995.

[54] S. Sharafkhani, M. Kokabi, Coaxially oriented PVDF/MWCNT nanofibers as a high-performance piezoelectric actuator, Polym. Compos. 44 (12) (2023) 8780–8791, https://doi.org/10.1002/pc.27736.

[55] P.K. Szewczyk, D.P. Ura, U. Stachewicz, Humidity controlled mechanical properties of electrospun polyvinylidene fluoride (PVDF) fibers, Fibers 8 (10) (2020), https://doi.org/10.3390/fib8100065.

[56] Y. Hong, B. Wang, Z. Long, Z. Zhang, Q. Pan, S. Liu, X. Luo, Z. Yang, Hierarchically interconnected piezoceramic textile with a balanced performance in piezoelectricity, flexibility, toughness, and air permeability, Adv. Funct. Mater. 31 (42) (2021) 2104737, https://doi.org/10.1002/adfm.202104737.

[57] Y. Si, J. Yang, D. Wang, S. Shi, C. Zhi, K. Huang, J. Hu, Bioinspired hierarchical multi-protective membrane for extreme environments via co-electrospinning-electrospray strategy, Small (2023) 2304705, https://doi.org/10.1002/smll.202304705.

[58] C. Tang, Z. Liu, Q. Hu, Z. Jiang, M. Zheng, C. Xiong, S. Wang, S. Yao, Y. Zhao, X. Wan, G. Liu, Q. Sun, Z.L. Wang, L. Li, Unconstrained piezoelectric vascular electronics for wireless monitoring of hemodynamics and cardiovascular health, Small (2023) 2304752, https://doi.org/10.1002/smll.202304752.

[59] N. Chand and M. Fahim, 1 - Natural fibers and their composites, in Tribology of Natural Fiber Polymer Composites (Second Edition), N. Chand and M. Fahim Eds.: Woodhead Publishing, 2021, pp. 1–59.

[60] H.-H. Kim, C.-G. Park, Plant growth and water purification of porous vegetation concrete formed of blast furnace slag, natural jute fiber and styrene butadiene latex, Sustainability 8 (4) (2016) 386, https://doi.org/10.3390/su8040386.

[61] C. Huang, N.L. Thomas, Fabrication of porous fibers via electrospinning: strategies and applications, Polym. Rev. 60 (4) (2020) 595–647, https://doi.org/10.1080/15583724.2019.1688830.

[62] Y. Liu, H. Liu, J. Xiong, A. Li, R. Wang, L. Wang, X. Qin, J. Yu, Bioinspired design of electrospun nanofiber based aerogel for efficient and cost-effective solar vapor generation, Chem. Eng. J. 427 (2022) 131539, https://doi.org/10.1016/j.cej.2021.131539.

[63] Y. Liao, R. Wang, A.G. Fane, Fabrication of bioinspired composite nanofiber membranes with robust superhydrophobicity for direct contact membrane distillation, Environ. Sci. Technol. 48 (11) (2014) 6335–6341, https://doi.org/10.1021/es405795s.

[64] D. Shen, Y. Liu, M. Yu, F. Kong, B. Xin, Y. Liu, Bioinspired flexible and highly responsive PVDF-based humidity sensors for respiratory monitoring, Polymer 254 (2022) 125103, https://doi.org/10.1016/j.polymer.2022.125103.

[65] Y. Su, T. Fan, H. Bai, H. Guan, X. Ning, M. Yu, Y. Long, Bioinspired superhydrophobic and superlipophilic nanofiber membrane with pine needle-like structure for efficient gravity-driven oil/water separation, Sep. Purif. Technol. 274 (2021) 119098, https://doi.org/10.1016/j.seppur.2021.119098.

[66] Y. Dou, X. Liu, K. Yu, X. Wang, W. Liu, J. Liang, C. Liang, Biomass porous carbon derived from jute fiber as anode materials for lithium-ion batteries, Diam. Relat. Mater. 98 (2019) 107514, https://doi.org/10.1016/j.diamond.2019.107514.

[67] M. Neumann, M.J. Lawes, Quantifying carbon in tree bark: the importance of bark morphology and tree size, Methods Ecol. Evol. 12 (4) (2021) 646–654, https://doi.org/10.1111/2041-210X.13546.

[68] P. Lu, Y. Xia, Maneuvering the internal porosity and surface morphology of electrospun polystyrene yarns by controlling the solvent and relative humidity, Langmuir 29 (23) (2013) 7070–7078, https://doi.org/10.1021/la400747y.

[69] C. Huang, N.L. Thomas, Fabricating porous poly(lactic acid) fibres via electrospinning, Eur. Polym. J. 99 (2018) 464–476, https://doi.org/10.1016/j.eurpolymj.2017.12.025.

[70] N.I. Nawi, N.R. Sait, M.R. Bilad, N. Shamsuddin, J. Jaafar, N.A. Nordin, T. Narkkun, K. Faungnawakij, D.F. Mohshim, Polyvinylidene fluoride membrane via vapour induced phase separation for oil/water emulsion filtration, Polymers 13 (3) (2021) 427, https://doi.org/10.3390/polym13030427.

[71] D. Chen, K. Chen, K. Brown, A. Hang, J.X.J. Zhang, Liquid-phase tuning of porous PVDF-TrFE film on flexible substrate for energy harvesting, Appl. Phys. Lett. 110 (15) (2017) 153902, https://doi.org/10.1063/1.4980130.

[72] W. Liu, C. Huang, X. Jin, Electrospinning of grooved polystyrene fibers: effect of solvent systems, Nanoscale Res. Lett. 10 (1) (2015) 237, https://doi.org/10.1186/s11671-015-0949-5.

[73] P. van de Witte, P.J. Dijkstra, J.W.A. van den Berg, J. Feijen, Phase separation processes in polymer solutions in relation to membrane formation, J. Membr. Sci. 117 (1) (1996) 1–31, https://doi.org/10.1016/0376-7388(96)00088-9.
[74] S. Liang, Y. Kang, A. Tiraferri, E.P. Giannelis, X. Huang, M. Elimelech, Highly hydrophilic polyvinylidene fluoride (PVDF) ultrafiltration membranes via postfabrication grafting of surface-tailored silica nanoparticles, ACS Appl. Mater. Interfaces 5 (14) (2013) 6694–6703, https://doi.org/10.1021/am401462e.
[75] J.R. Gregorio, M. Cestari, Effect of crystallization temperature on the crystalline phase content and morphology of poly(vinylidene fluoride), J. Polym. Sci. Part B: Polym. Phys. 32 (5) (1994) 859–870, https://doi.org/10.1002/polb.1994.090320509.
[76] L. Ruan, X. Yao, Y. Chang, L. Zhou, G. Qin, X. Zhang, Properties and applications of the β phase poly(vinylidene fluoride), Polymers 10 (3) (2018) 228, https://doi.org/10.3390/polym10030228.
[77] M.M. Abolhasani, M. Naebe, M. Hassanpour Amiri, K. Shirvanimoghaddam, S. Anwar, J.J. Michels, K. Asadi, Hierarchically structured porous piezoelectric polymer nanofibers for energy harvesting, Adv. Sci. 7 (13) (2020) 2000517, https://doi.org/10.1002/advs.202000517.
[78] I. Miranda, A. Souza, P. Sousa, J. Ribeiro, E.M.S. Castanheira, R. Lima, G. Minas, Properties and applications of PDMS for biomedical engineering: a review, J. Funct. Biomater. 13 (1) (2021) 2, https://doi.org/10.3390/jfb13010002.
[79] H. Zhan, Y.W. Chen, Q.Q. Shi, Y. Zhang, R.W. Mo, J.N. Wang, Highly aligned and densified carbon nanotube films with superior thermal conductivity and mechanical strength, Carbon 186 (2022) 205–214, https://doi.org/10.1016/j.carbon.2021.09.069.
[80] D. Chen, T. Sharma, J.X.J. Zhang, Mesoporous surface control of PVDF thin films for enhanced piezoelectric energy generation, Sens. Actuators A: Phys. 216 (2014) 196–201, https://doi.org/10.1016/j.sna.2014.05.027.
[81] O.Y. Ol'khovik, E.S. Grigoryan, Apparatus for measuring compressibility of polymers, Polym. Sci. U. S. S. R. 16 (9) (1974) 2501–2506, https://doi.org/10.1016/0032-3950(74)90257-3.
[82] G. Lee, M. Zarei, Q. Wei, Y. Zhu, S.G. Lee, Surface wrinkling for flexible and stretchable sensors, Small 18 (42) (2022) 2203491, https://doi.org/10.1002/smll.202203491.
[83] A. Kumar, A. Kumar, K. Prasad, Energy harvesting from ceramic/blended polymer nanocomposites: Ba0.85Ca0.15Zr0.10Ti0.90O3/polyvinylidene fluoride–polytetrafluoroethylene, Phys. Status Solidi (a) 218 (20) (2021) 2100382, https://doi.org/10.1002/pssa.202100382.
[84] M.-H. You, X.-X. Wang, X. Yan, J. Zhang, W.-Z. Song, M. Yu, Z.-Y. Fan, S. Ramakrishna, Y.-Z. Long, A self-powered flexible hybrid piezoelectric–pyroelectric nanogenerator based on non-woven nanofiber membranes, J. Mater. Chem. A 6 (8) (2018) 3500–3509, https://doi.org/10.1039/C7TA10175A.
[85] Z. Lu, C. Zhang, S.H. Kwon, Z. Jiang, L. Dong, Flexible hybrid piezoelectric-electrostatic device for energy harvesting and sensing applications, Adv. Mater. Interfaces 10 (8) (2023) 2202173, https://doi.org/10.1002/admi.202202173.
[86] M.A. Islam, K. Sundaraj, R.B. Ahmad, N.U. Ahamed, Mechanomyogram for muscle function assessment: a review, PLOS One vol. 8 (3) (2013) e58902, https://doi.org/10.1371/journal.pone.0058902.
[87] W.W. Nichols, Clinical measurement of arterial stiffness obtained from noninvasive pressure waveforms, American Journal of Hypertension, vol. 18, no. S1, pp. 3S–10S, 2005, doi: 10.1016/j.amjhyper.2004.10.009.
[88] A. Taebi, B.E. Solar, A.J. Bomar, R.H. Sandler, H.A. Mansy, Recent advances in seismocardiography, Vibration 2 (1) (2019) 64–86, https://doi.org/10.3390/vibration2010005.
[89] A. Akhbardeh, K. Tavakolian, V. Gurev, T. Lee, W. New, B. Kaminska, and N. Trayanova, Comparative analysis of three different modalities for characterization of the seismocardiogram, Annu Int Conf IEEE Eng Med Biol Soc, vol. 2009, pp. 2899–903, 2009, doi: 10.1109/iembs.2009.5334444.
[90] C. Yang, S. Tang, and N. Tavassolian, Annotation of seismocardiogram using gyroscopic recordings, In: Proceedings of the 2016 IEEE Biomedical Circuits and Systems Conference (BioCAS), 2016, pp. 204–207, doi: 10.1109/BioCAS.2016.7833767.
[91] P. Dehkordi, E.P. Bauer, K. Tavakolian, V. Zakeri, A.P. Blaber, F. Khosrow-Khavar, Identifying patients with coronary artery disease using rest and exercise seismocardiography, Front. Physiol. 10 (2019) 1211, https://doi.org/10.3389/fphys.2019.01211.
[92] P. Sahoo, H. Thakkar, W.-Y. Lin, P.-C. Chang, M.-Y. Lee, On the design of an efficient cardiac health monitoring system through combined analysis of ECG and SCG signals, Sensors 18 (2) (2018) 379, https://doi.org/10.3390/s18020379.

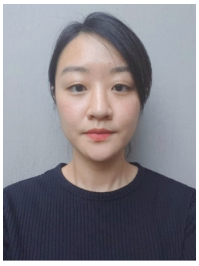

Sun Hwa Kwon is a PhD student under the supervision of Professor Lin Dong at New Jersey Institute of Technology. She received her undergraduate and M.S. degrees from The Cooper Union for the Advancement of Science and Art. Her research interests include nanofibers, specifically piezoelectric nanofibers created using the electrospinning fabrication method, and biomedical devices, such as cardiac devices.

Chi Zhang is currently a postdoctoral research associate under the supervision of Professor Lin Dong at New Jersey Institute of Technology. He received his Ph.D. from Technical Institute of Physics and Chemistry, Chinese Academy of Sciences. His research interests include functional nanomaterials and flexible electronics for sensing and energy harvesting applications.

Zhipeng Jiang is a PhD student at NJIT under thesupervision of Professor Lin Dong at New Jersey Institute of Technology. Hereceived her undergraduate and M.S. degrees from the University of Dayton forScience in Mechanical Engineering. His research interests include soft roboticsand flexible sensors-enabled digital health systems.

Lin Dong is an Assistant Professor at Department of Mechanical & Industrial Engineering at New Jersey Institute of Technology. She received her Ph.D. from Stevens Institute of Technology, where she was awarded Innovation and Entrepreneurship Doctoral Fellowship. She was a Research Associate at Thayer School of Engineering at Dartmouth College. Her research interests include nanomaterials and nanofabrication technology, flexible electronics, as well as energy harvesting and sensing devices for biomedical applications.